

Full Length Article

On the conversion of point-to-linear hierarchical micro/nano-structures on the glassy carbon surface by nanosecond pulsed laser irradiation

Chao Wang^a, Hongyang Zhang^a, Hu Huang^{a,*}, Zhiyu Zhang^b, Lin Zhang^c, Jiwang Yan^c

^a Key Laboratory of CNC Equipment Reliability, Ministry of Education, School of Mechanical and Aerospace Engineering, Jilin University, Changchun, Jilin 130022, China

^b Key Laboratory of Optical System Advanced Manufacturing Technology, Changchun Institute of Optics, Fine Mechanics and Physics, Chinese Academy of Sciences, Changchun, People's Republic of China

^c Department of Mechanical Engineering, Faculty of Science and Technology, Keio University, Yokohama 223-8522, Japan

ARTICLE INFO

Keywords:

Glassy carbon
Nanosecond pulsed laser
Conversion
Hierarchical micro/nano-structures

ABSTRACT

Fabrication of microstructures on the glassy carbon (GC) surface is crucial for its functional applications. However, due to its intrinsic mechanical, physical, and chemical properties, it is still challenging to fabricate hierarchical micro/nano-structures on the GC surface. In this study, by tuning the interval between adjacent points as well as the irradiation time, the conversion from the point to linear hierarchical micro/nano-structures was successfully achieved on the GC surface by nanosecond pulsed laser irradiation. The detailed conversion process and mechanism were explored and discussed. On this basis, the linear hierarchical micro/nano-structures were fabricated by direct line scanning, and the internal nanostructures were always parallel to the laser scanning direction. By repeated line scanning with relatively low laser fluence, the method of direct line scanning was further improved, and well-defined and uniform hierarchical micro/nano-structures were fabricated.

1. Introduction

As a kind of renewable material, glassy carbon (GC) possesses versatile mechanical, physical, and chemical properties, such as good impermeability of gas and liquid, excellent electrical conductivity, chemical inertness, and biocompatibility [1–3]. With these features, GC is an alternative for various technological applications, including (I) protection materials for ablative shielding [4], nuclear waste storage [5], and chemical reactions [6], (II) electrochemical devices for sensors [7] and energy storage [8], and (III) biomedical implants [9]. More interestingly, due to outstanding mechanical strength and thermal stability, GC is also a suitable option for the mold material of different metals and glasses [10–12]. Furthermore, with the aid of precision molding technology, high-precision optical [13] and microfluidic devices [14] with complex geometric structures could be fabricated. However, constructing suitable microstructures on the GC surface is a prerequisite for these processes, which will directly affect the performance of the molded devices. Therefore, it is essential for preparing the microstructures on the GC surface.

Nowadays, it is still challenging to obtain defect-free micro/nano-structures with complex geometry on the GC surface. By those

conventional processing methods [1], surface defects are easily generated on the GC surface due to its hard and brittle properties determined by the ‘glass’ nature of GC. Therefore, some alternative strategies have been developed, such as electron beam lithography (EBL) with reactive ion etching (RIE) [15], carbonization of cured resin [16], and laser processing [17]. Although surface microstructures with high precision and surface finish have been fabricated by the above strategies, they are still limited by simple geometries. Previous studies have demonstrated that hierarchical micro/nano-structures may endow superior performance to the material surfaces than these simple structures, for example, enhanced light absorption efficiency [18,19], tunable surface wettability [20,21], and improved tribological properties [22]. However, the difficulty of fabricating hierarchical micro/nano-structures is also significantly increased, and until now, very few studies have reported the fabrication of hierarchical micro/nano-structures on the GC surface.

In our recent research [23], a typical hierarchical micro/nano-structures (micro-dimple with ring-like nanostructures on its inner wall) was produced on the GC surface by using a nanosecond pulsed laser. However, it is still limited to a single-point process with low flexibility and efficiency, which may hinder the widespread application of this method. Accordingly, in this study, it was attempted to fabricate

* Corresponding author.

E-mail address: huanghu@jlu.edu.cn (H. Huang).

linear hierarchical micro/nano-structures on the GC surface by the point-to-linear conversion. By tuning the interval between adjacent points as well as the irradiation time, well-defined and uniform linear hierarchical micro/nano-structures were successfully achieved on the GC surface. The detailed conversion process and mechanism from the point to linear hierarchical micro/nano-structures were explored and discussed.

2. Materials and experiments

The polished glassy carbon was purchased from UNITIKA LTD., Japan, as the experimental sample in this study. A fiber nanosecond pulsed system (SP-050P-A-EP-Z-F-Y, SPI, UK) (laser wavelength: 1064 nm, pulse width: 7 ns, repetition frequency: 700 kHz, laser beam diameter: $\sim 42 \mu\text{m}$) was employed to fabricate the hierarchical micro/nano-structures on the GC surface. The laser energy has a Gaussian distribution (TEM₀₀ mode, $M^2 < 1.6$).

In the previous study [23], a typical point-shape hierarchical micro/nano-structure (micro-dimple with ring-like nanostructures on its inner wall) has been reported on the GC surface, but it is still uncharted whether the linear hierarchical micro/nano-structures could be developed on this basis. When the laser fluence is 0.235 J/cm^2 and irradiation time is 1.0 ms, the generated point-shape hierarchical micro/nano-structure is well-defined and it has a depth of $7.65 \mu\text{m}$ and diameter of $24.5 \mu\text{m}$. Accordingly, to investigate the conversion process from the point to linear hierarchical micro/nano-structures, the interval (d) between adjacent points is reduced and the laser fluence is kept to be 0.235 J/cm^2 . However, according to some pre-experimental results, the laser-induced structures are easily damaged by the thermal accumulation due to the reduction of the interval. Therefore, to obtain well-defined structures, the irradiation time (t) is also reduced correspondingly. By analyzing the pre-experimental results, the laser parameters as shown in the yellow regions of Fig. 1 are selected for exploring the conversion process. Under these laser parameters, some representative and distinguishable structures could be formed on the irradiated surface.

After laser irradiation, the laser-irradiated surfaces were observed by using the scanning electron microscope (SEM, JSM-IT500A, JEOL, Japan) and the laser scanning confocal microscope (LSCM, OLS4100, Olympus, Japan). During SEM observation, the acceleration voltage, current, and working distance (WD) were 5.0 kV, 3.0 mA, and 10.1 mm, respectively. The amorphous nature of GC surface before and after laser irradiation was characterized by laser micro-Raman spectroscopy (NRS-3100, JASCO, Japan) with a 532 nm wavelength laser.

3. Results and discussion

3.1. Conversion of point-to-linear hierarchical micro/nano-structures

Fig. 2 presents the SEM morphologies of laser irradiated GC surfaces after multiple-point shots, and the conversion process of surface microstructures could be clearly observed. For all these experiments, the laser fluence is kept to be 0.235 J/cm^2 . By the pre-experimental results, the diameter of an individual micro-dimple is about $24 \mu\text{m}$ when the irradiation time is 1.0 ms. Therefore, at a relatively large interval of $22 \mu\text{m}$ or $20 \mu\text{m}$, no obvious interaction between adjacent micro-dimples appears, and the individual micro-dimple still keeps the initial morphology. When the interval is between $14 \sim 18 \mu\text{m}$, two adjacent micro-dimples gradually overlap as the interval decreases, and a clear boundary could be observed in the overlapping region (Fig. 2c). In this case, the individual micro-dimple could still be distinguished, but the branches inside the micro-dimple initially form and gradually develop along with three directions (Fig. 2d). And the internal nanostructures are gradually concentrated at the branches rather than uniformly distributed with the initial ring-like shape. Furthermore, as shown in Fig. 2e, some grid arrays are generated on the inner wall of the micro-dimple by the intersecting nanostructures. Meanwhile, some nanoparticles also begin to deposit on two sides of the micro-dimple.

When decreasing the interval to $12 \mu\text{m}$ (Fig. 2f), the boundary between two adjacent micro-dimples is broken by interconnecting branches, failing to keep the individual micro-dimple morphology. The internal nanostructures in the overlapping regions begin to interconnect along the x -direction. And more and more nanoparticles are deposited on the surface of micro-dimples and internal nanostructures, which seriously affects the observation of these structures. Therefore, at the same interval of $12 \mu\text{m}$, the irradiation time is shortened to 0.8 ms to distinguish these microstructures (Fig. 2g). When the interval gradually decreases from $12 \mu\text{m}$ to $8 \mu\text{m}$, the branches along the y -direction further develop towards two sides of the micro-dimple. While the internal nanostructures being parallel to the x -direction are connected more closely, and more nanoparticles are covered on the branches and nanostructures, as shown in Fig. 2g–i. As shown in Fig. 2j–l, when the irradiation time is further shortened to 0.6 ms, uniform linear grooves instead of distinguishable micro-dimples are generated as the interval reduces to $4 \sim 8 \mu\text{m}$. Meanwhile, the internal nano-gratings being parallel to the x -direction replace the initial ring-like structures and further develop to the outsides of the grooves. From the above results, it is indicated that the conversion from the point to linear hierarchical micro/nano-structures could be successfully achieved by tuning the interval between adjacent points as well as the irradiation time.

To further analyze the conversion process, the typical three-dimensional (3D) topographies of laser irradiated GC surfaces as well as the corresponding cross-sectional profiles along the x -direction are presented in Fig. 3. The applied laser parameters are identical to those in Fig. 2. When the interval is between $14 \sim 20 \mu\text{m}$, the smooth stages (marked in Fig. 3b) could always be observed on the cross-sectional profiles of the micro-dimples, which may be related to the boundary regions between adjacent micro-dimples. It is noticeable that when the interval is reduced to $12 \mu\text{m}$, the smooth stages of the cross-sectional profiles disappear, which is consistent with the boundary broken by the interconnecting branches in Fig. 2f. As shown in Fig. 3d, when the interval decreases from $12 \mu\text{m}$ to $8 \mu\text{m}$, the fluctuating cross-sectional profiles gradually become steady under the irradiation time of 0.8 ms, proving that the micro-dimples are more closely connected in Fig. 2g–i. When the interval is between $4 \sim 8 \mu\text{m}$ (Fig. 3f), the cross-sectional profiles along the x -direction maintain a relatively stable linear shape under the irradiation time of 0.6 ms, which is closely related to the SEM morphologies of the formed linear grooves (Fig. 2j–l).

According to the above experimental results and analysis, the conversion mechanism from the point to linear hierarchical micro/nano-structures would be comprehensively discussed. First, by the previous study [23], the evolution of the hierarchical micro/nano-structures after the single-point shot is illustrated in Fig. 4a. When increasing the irradiation time or laser fluence, the ring-like nanostructures in the center of the micro-dimple deteriorate and become disordered, and the branches with different lengths extend outward in arbitrary five directions. This may be due to the more efficient absorption of laser energy in the 'weak' ('weak' means more defects or worse surface quality) directions of the central region [24]. Further increasing the irradiation time or laser fluence, the new ring-like nanostructures are generated in the center of the micro-dimple, and the surrounding branches also further develop

When decreasing the interval to $12 \mu\text{m}$ (Fig. 2f), the boundary between two adjacent micro-dimples is broken by interconnecting branches, failing to keep the individual micro-dimple morphology. The internal nanostructures in the overlapping regions begin to interconnect along the x -direction. And more and more nanoparticles are deposited on the surface of micro-dimples and internal nanostructures, which seriously affects the observation of these structures. Therefore, at the same interval of $12 \mu\text{m}$, the irradiation time is shortened to 0.8 ms to distinguish these microstructures (Fig. 2g). When the interval gradually decreases from $12 \mu\text{m}$ to $8 \mu\text{m}$, the branches along the y -direction further develop towards two sides of the micro-dimple. While the internal nanostructures being parallel to the x -direction are connected more closely, and more nanoparticles are covered on the branches and nanostructures, as shown in Fig. 2g–i. As shown in Fig. 2j–l, when the irradiation time is further shortened to 0.6 ms, uniform linear grooves instead of distinguishable micro-dimples are generated as the interval reduces to $4 \sim 8 \mu\text{m}$. Meanwhile, the internal nano-gratings being parallel to the x -direction replace the initial ring-like structures and further develop to the outsides of the grooves. From the above results, it is indicated that the conversion from the point to linear hierarchical micro/nano-structures could be successfully achieved by tuning the interval between adjacent points as well as the irradiation time.

To further analyze the conversion process, the typical three-dimensional (3D) topographies of laser irradiated GC surfaces as well as the corresponding cross-sectional profiles along the x -direction are presented in Fig. 3. The applied laser parameters are identical to those in Fig. 2. When the interval is between $14 \sim 20 \mu\text{m}$, the smooth stages (marked in Fig. 3b) could always be observed on the cross-sectional profiles of the micro-dimples, which may be related to the boundary regions between adjacent micro-dimples. It is noticeable that when the interval is reduced to $12 \mu\text{m}$, the smooth stages of the cross-sectional profiles disappear, which is consistent with the boundary broken by the interconnecting branches in Fig. 2f. As shown in Fig. 3d, when the interval decreases from $12 \mu\text{m}$ to $8 \mu\text{m}$, the fluctuating cross-sectional profiles gradually become steady under the irradiation time of 0.8 ms, proving that the micro-dimples are more closely connected in Fig. 2g–i. When the interval is between $4 \sim 8 \mu\text{m}$ (Fig. 3f), the cross-sectional profiles along the x -direction maintain a relatively stable linear shape under the irradiation time of 0.6 ms, which is closely related to the SEM morphologies of the formed linear grooves (Fig. 2j–l).

According to the above experimental results and analysis, the conversion mechanism from the point to linear hierarchical micro/nano-structures would be comprehensively discussed. First, by the previous study [23], the evolution of the hierarchical micro/nano-structures after the single-point shot is illustrated in Fig. 4a. When increasing the irradiation time or laser fluence, the ring-like nanostructures in the center of the micro-dimple deteriorate and become disordered, and the branches with different lengths extend outward in arbitrary five directions. This may be due to the more efficient absorption of laser energy in the 'weak' ('weak' means more defects or worse surface quality) directions of the central region [24]. Further increasing the irradiation time or laser fluence, the new ring-like nanostructures are generated in the center of the micro-dimple, and the surrounding branches also further develop

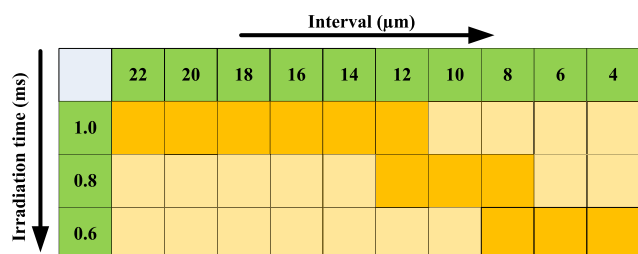


Fig. 1. The laser parameters selected in this study.

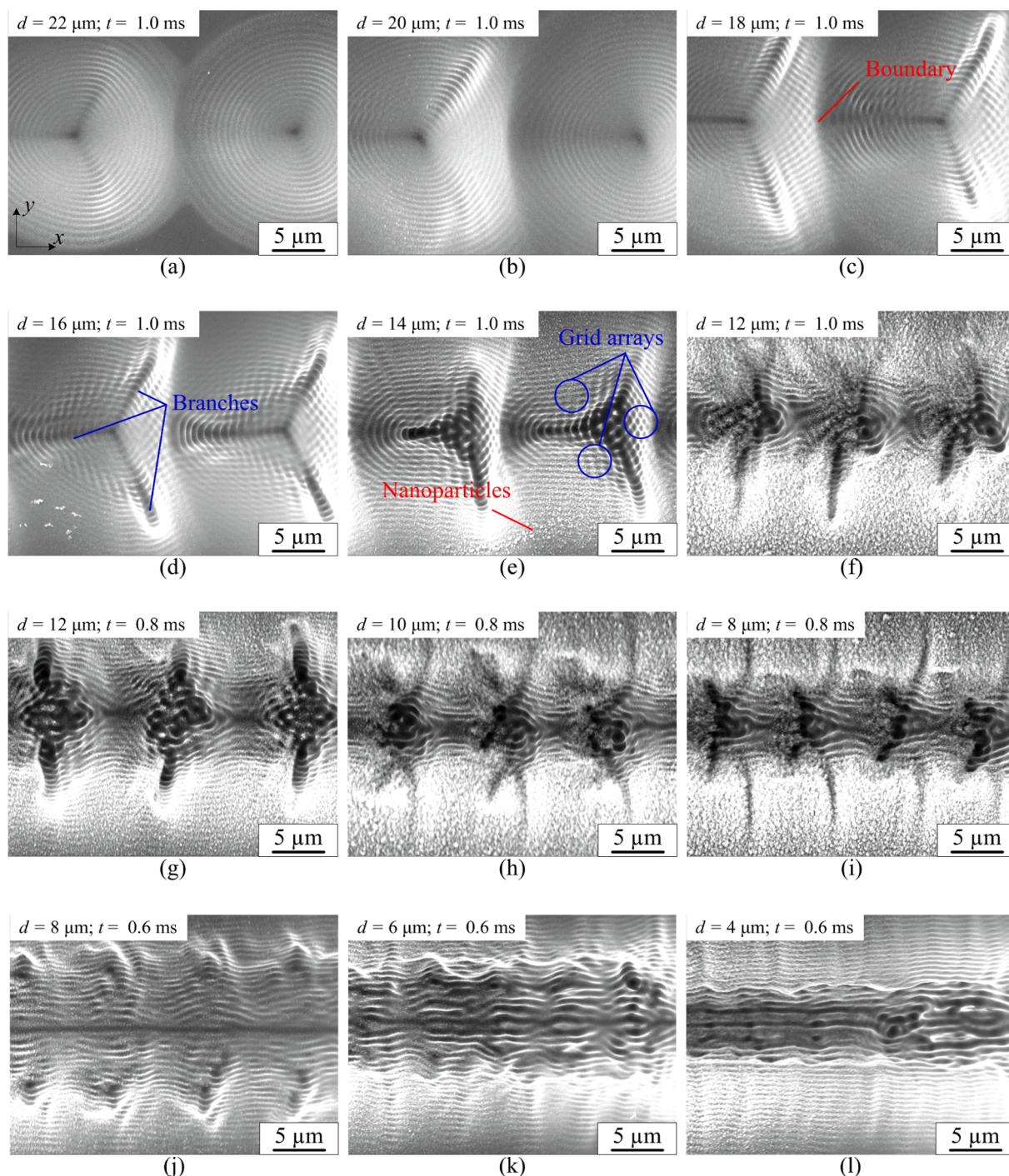


Fig. 2. SEM morphologies of laser irradiated GC surfaces after multiple-point shots under the applied laser parameters: (a) $d = 22 \mu\text{m}$, (b) $d = 20 \mu\text{m}$, (c) $d = 18 \mu\text{m}$, (d) $d = 16 \mu\text{m}$, (e) $d = 14 \mu\text{m}$, and (f) $d = 12 \mu\text{m}$ at the irradiation time of 1.0 ms; (g) $d = 12 \mu\text{m}$, (h) $d = 10 \mu\text{m}$, and (i) $d = 8 \mu\text{m}$ at the irradiation time of 0.8 ms; (j) $d = 8 \mu\text{m}$, (k) $d = 6 \mu\text{m}$, and (l) $d = 4 \mu\text{m}$ at the irradiation time of 0.6 ms. For all these experiments, the laser fluence is kept to be 0.235 J/cm^2 .

outward.

However, when the multiple-point shots are performed, the evolution process of these structures becomes complicated. Since two representative features could be observed in the conversion process, i.e. the branch and the internal nanostructure, their evolution will be discussed separately, which are illustrated in Fig. 4b and c. As shown in Fig. 4b, at a relatively large interval of $22 \mu\text{m}$ or $20 \mu\text{m}$, the interaction between two adjacent micro-dimples is very weak. When the interval is between $12 \sim 18 \mu\text{m}$, the branches along three directions (A, B, and C) are produced on the inner surface of each micro-dimple. Among them, the

branch-A is formed along the x-direction in the center of the micro-dimple (Fig. 4b) because of the relatively high laser energy in the central region as well as the effect of the preceding shot. Actually, its direction depends on the position of the subsequent multiple-point shots, and it is always parallel to the scanning direction, which would be confirmed in the subsequent experiments. Compared to the surrounding regions after the single-point shot, the interfaces (Fig. 4b) of adjacent micro-dimples are relatively 'weak', so the absorption of laser energy is more effective, leading to the formation of branch-B and branch-C. Therefore, their direction is related to the positions of the interfaces,

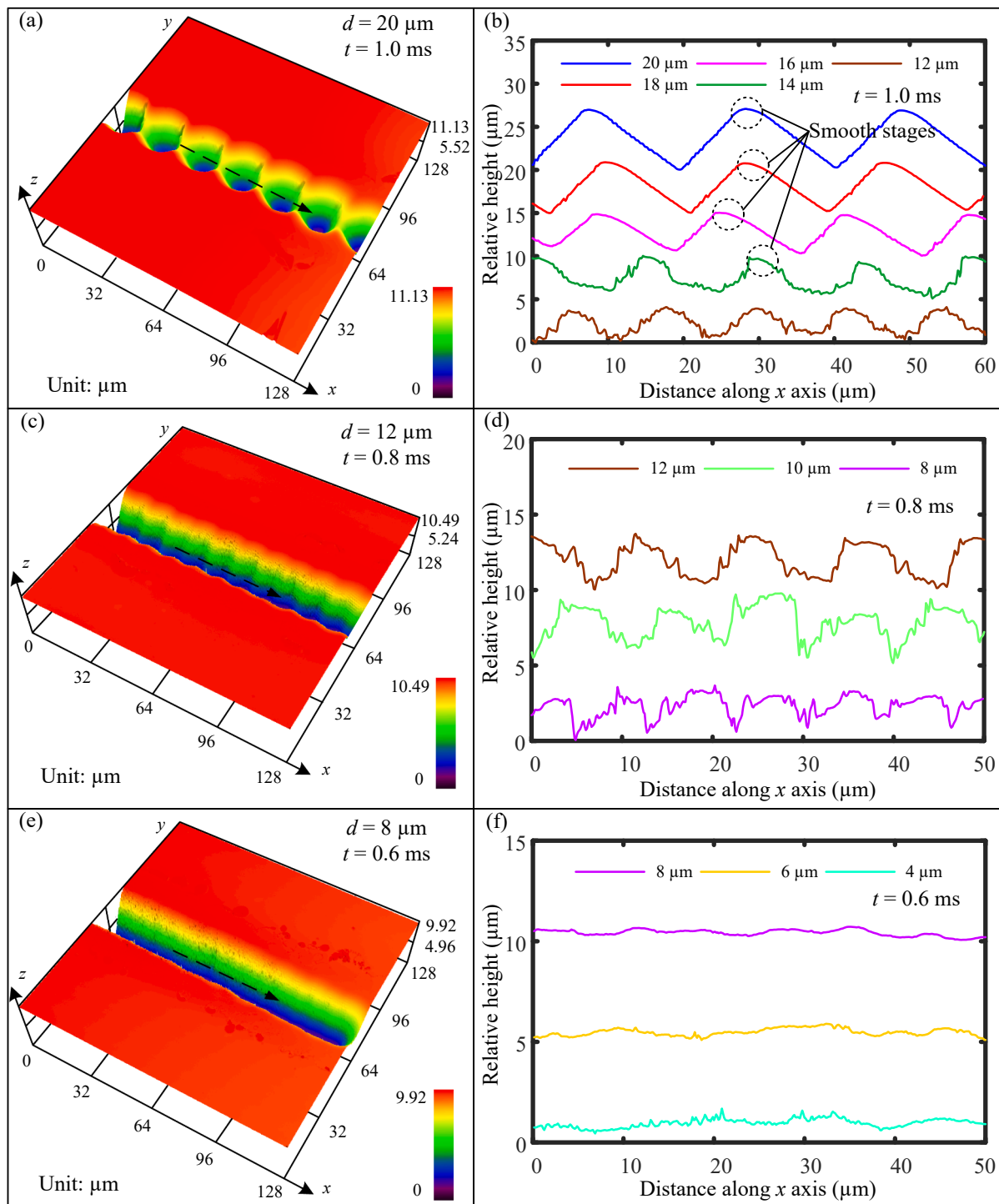


Fig. 3. The typical 3D topographies of laser irradiated GC surfaces under various intervals between adjacent points and irradiation times: (a) $d = 20 \mu\text{m}$, $t = 1.0 \text{ ms}$; (c) $d = 12 \mu\text{m}$, $t = 0.8 \text{ ms}$; (e) $d = 8 \mu\text{m}$, $t = 0.6 \text{ ms}$. (b), (d), and (f) The cross-sectional profiles along the x -direction under the laser parameters corresponding to those in Fig. 2.

corresponding to the tangential direction of the interfaces of the next micro-dimple. Accordingly, when decreasing the interval, the positions of the interfaces between adjacent micro-dimples would change, so the angle θ between branch-B and branch-C also increases in Fig. 2c–e. When the interval is the radius ($12 \mu\text{m}$) of the micro-dimple, the boundaries of adjacent micro-dimples are broken by the interconnecting branches-A. Meanwhile, the angle θ between branch-B and branch-C reaches a maximum value of 180° , and two branches are parallel to

the y -direction. Therefore, further decreasing the interval to $8 \sim 12 \mu\text{m}$, the interconnecting branches-A constitute the central region of the groove in Fig. 2g–i. When the interval reduces to $4 \sim 8 \mu\text{m}$, the adjacent branches-B or branches-C are also interconnected, forming the outer region of the regular linear groove in Fig. 2j–l.

According to the experimental results, the evolution of internal nanostructures is related to the formation of branches. Similarly, at a relatively large interval of 20 or $22 \mu\text{m}$, the internal ring-like

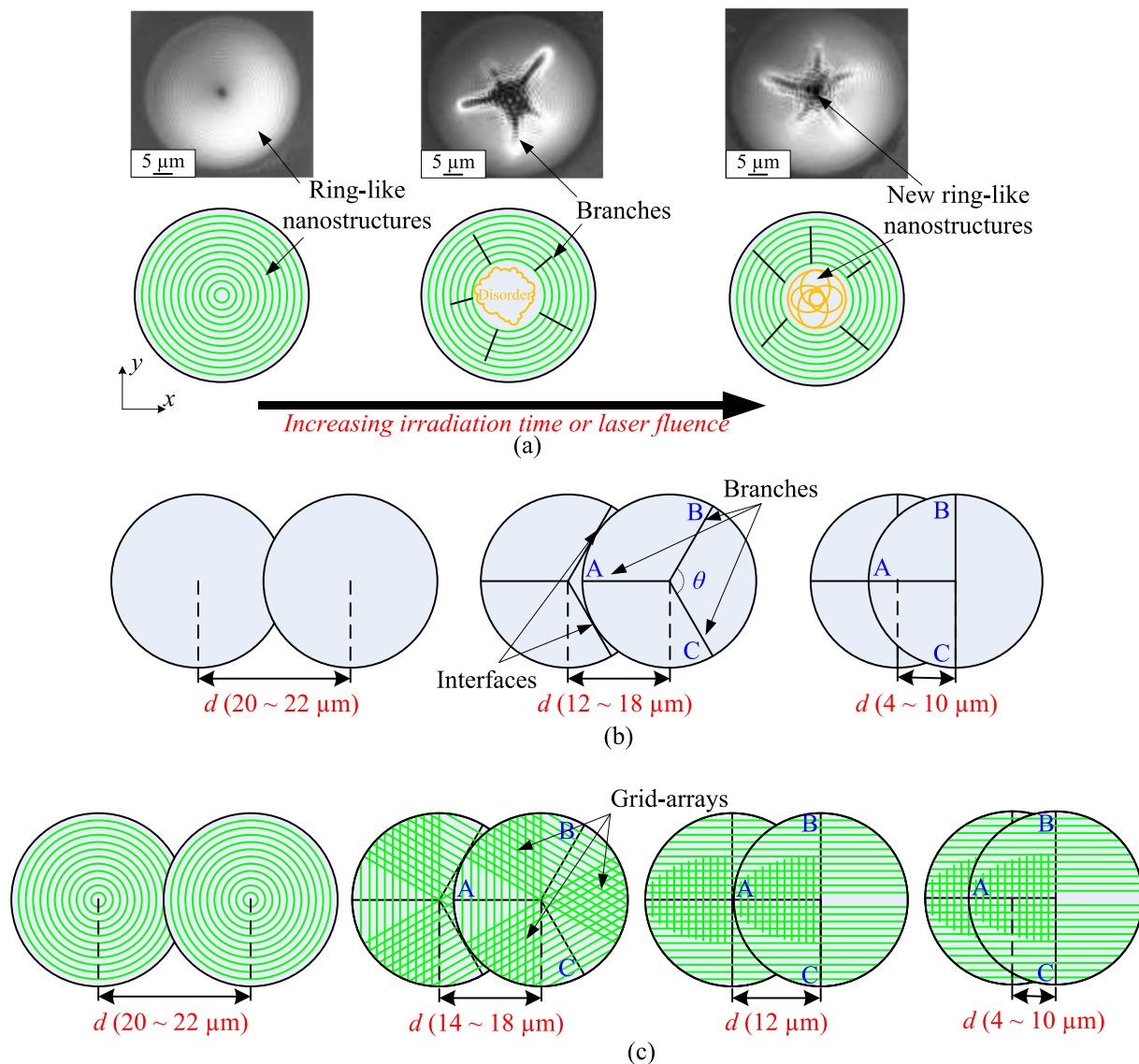


Fig. 4. The schematic diagrams illustrating the evolution of micro/nano-structures: (a) point-shape hierarchical micro/nano-structures, (b) branch, and (c) internal nanostructure.

nanostructures are very weakly affected. But when the interval reduces to 14 ~ 18 μm, three branches are formed and gradually develop, with the internal nanostructures concentrated at the branches and distributed perpendicularly to them. As the interval decreases from 18 μm to 14 μm, the branch-A is always parallel to the x -direction and the angle θ between branch-B and branch-C gradually increases. Therefore, the distribution of nanostructures also changes with the development of branches. For example, as shown in Fig. 2d and e, the nanostructures guided by different branches intersect each other and form the grid arrays at the junction of branches. Furthermore, the effect of thermal accumulation on the GC surface morphology is also non-negligible, which leads to an increasing number of nanoparticles covering the irradiated region.

When the interval reduces to 12 μm, the adjacent branches-A have interconnected along the x -direction, and the branch-B and branch-C are also parallel to the y -direction. As a result, the internal nanostructures guided by the branch-B and branch-C are distributed along the x -direction and connected by interconnecting branches-A, which leads to the formation of parallel nanostructures. When the interval decreases from 12 μm to 8 μm (Fig. 2g-i), laser energy is absorbed more efficiently on the two sides of the irradiated region due to the massive ablation of

materials in the center of the irradiated region, further promoting the development of branch-B and branch-C. Therefore, with the decrease of the interval, the morphology of branch-A is almost unchanged, and the branch-B and branch-C gradually expand outwards. And the internal nanostructures being perpendicular to the branch-B and branch-C are more closely connected and play a dominant role in the overall nanostructures. As shown in Fig. 2j-l, at the relatively small interval of 4 ~ 8 μm, the nano-gratings along the x -direction are well achieved in the outer region of the linear groove. Noticeably, no regular nano-gratings are generated in the central regions of the groove due to the injection of more laser energy. According to the above analysis, the conversion mechanism from the point to linear hierarchical micro/nano-structures is related to the evolution of the branch and the internal nanostructure, which originates from the non-uniform absorption of laser energy on the GC surface.

3.2. Fabrication of linear hierarchical micro/nano-structures by direct line scanning

The above experimental results show that by changing the interval between adjacent points as well as the irradiation time, the linear

hierarchical micro/nano-structures have been well achieved through the multiple-point shots. However, the efficiency of producing the linear structures by the point shot processing is relatively low. Compared to the point shot processing, the direct line scanning is similar in theory, but it is more convenient and efficient in practical engineering. For example, when fabricating a linear hierarchical micro/nano-structures with the same length, the time by point shot processing is 4 ~ 5 times longer than that by direct line scanning. Therefore, the direct line scanning is attempted to fabricate the linear hierarchical micro/nano-structures on the GC surface. Fig. 5 presents the SEM morphologies and 3D topography by direct line scanning. It is worth noting that the interval between adjacent points is less than $0.04 \mu\text{m}$ under the laser frequency of 700 kHz and scanning speed of 25 mm/s. At such a small interval, the well-defined linear hierarchical micro/nano-structures could be well achieved, and these structures have a more uniform transition from two sides to the center of the scanning line, but it still has some shortcomings.

On the one hand, it can be concluded from Fig. 5a–c that the morphology of the nano-gratings is significantly different in various regions of the scanning line. For the starting region, the generated shallow nano-gratings are covered by deposited nanoparticles; while for the middle region and ending region, more distinguishable nano-gratings could be observed. Besides, in Fig. 5d–f, the cross-sectional profile along the y-axis shows uniform morphology, but the cross-sectional profile along the x-axis has regular fluctuation and deviation (Δh) in the height direction. These features could be attributed to the thermal accumulation of laser processing [25,26], which indicates that the morphology of linear hierarchical micro/nano-structures by direct line scanning is easily affected by the thermal effect. On the other hand, generally speaking, the surface topography of laser processing mainly depends on the laser fluence, followed by the scanning speed [27,28]. Fig. 6 presents the SEM morphologies in the middle regions of the scanning line obtained under various scanning speeds. When changing the scanning speed, the morphologies of linear hierarchical micro/nano-structures are significantly affected, which indicates that their

morphologies are sensitive to the changes in laser parameters. The above shortcomings would be further improved in section 3.3.

According to the conversion mechanism discussed in section 3.1, the direction of linear hierarchical micro/nano-structures including the linear groove and nano-gratings, depends on the direction of the branch, which is further determined by the position of the subsequent shots. Therefore, the direction of these micro/nano-structures could be flexibly controlled by adjusting the laser scanning path in theory, which is crucial for constructing some complex geometric patterns. To evaluate the patterning capacity of these micro/nano-structures, two different geometries, hexagon and helix, are fabricated on the GC surfaces. Figs. 7 and 8 present their SEM morphologies. As shown in Fig. 7, the direction of the linear groove and nano-gratings is always parallel to the laser scanning direction in various regions such as regions A, B, and C. In Fig. 8, the direction of the groove and nano-gratings could maintain the well helical shape as well. Furthermore, it is clearly seen that these micro/nano-structures share similar morphologies in various regions except for the starting and ending points. The above results demonstrate that the direction of linear hierarchical micro/nano-structures could be flexibly controlled by adjusting the laser scanning path, proving the great potential for patterning the GC surface.

3.3. Quality improvement of linear hierarchical micro/nano-structures by repeated line scanning

Although the linear hierarchical micro/nano-structures could be fabricated by direct line scanning, some shortcomings such as the difference in overall morphology and sensitivity of laser parameters, would hinder its practical application. Compared to direct line scanning, repeated line scanning with relatively low laser fluence can significantly reduce the effect of thermal accumulation on the overall morphology [29]. Therefore, this method is employed to improve the surface quality of the linear hierarchical micro/nano-structures. Fig. 9 presents the corresponding SEM morphologies and 3D topography by repeated line scanning. Compared to the SEM morphologies in Fig. 5, the

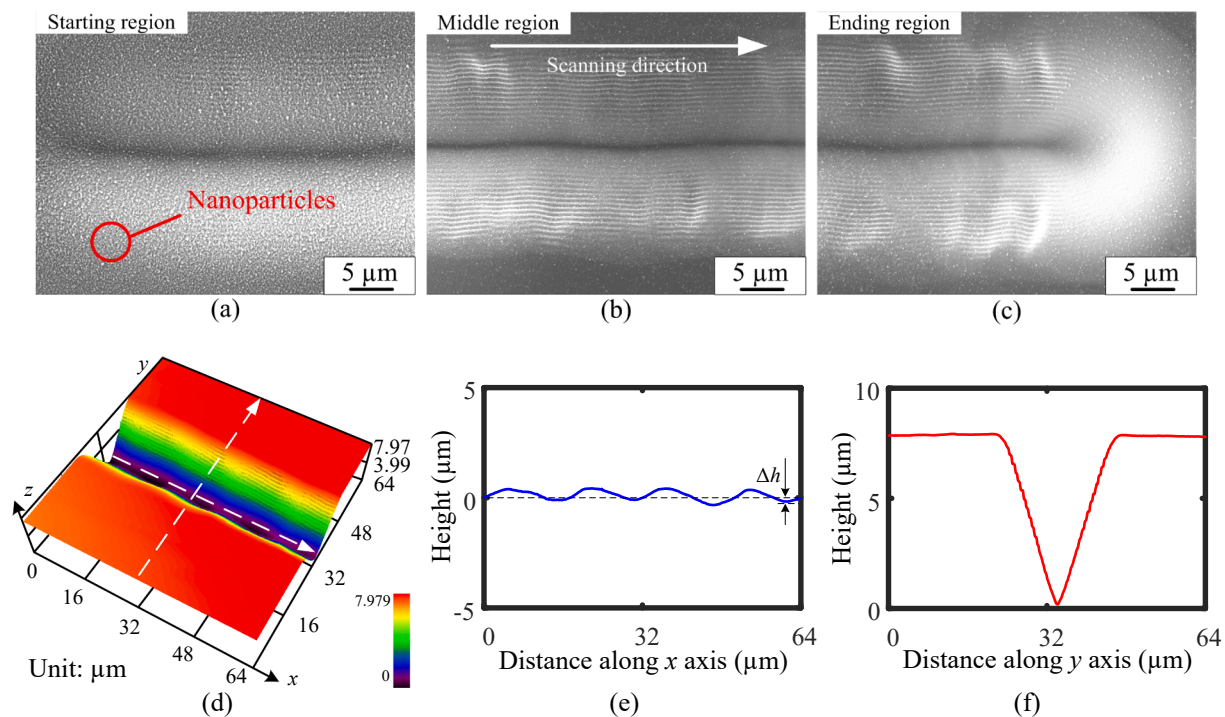


Fig. 5. SEM morphologies of laser irradiated GC surfaces in various regions of the scanning line by direct line scanning: (a) starting region, (b) middle region, and (c) ending region. (d) The 3D topography corresponds to the middle region of Fig. 5b and the cross-sectional profiles marked in Fig. 5d along different axes: (e) x-axis, (f) y-axis. The laser fluence and scanning speed are kept to be 0.235 J/cm^2 and 25 mm/s, respectively.

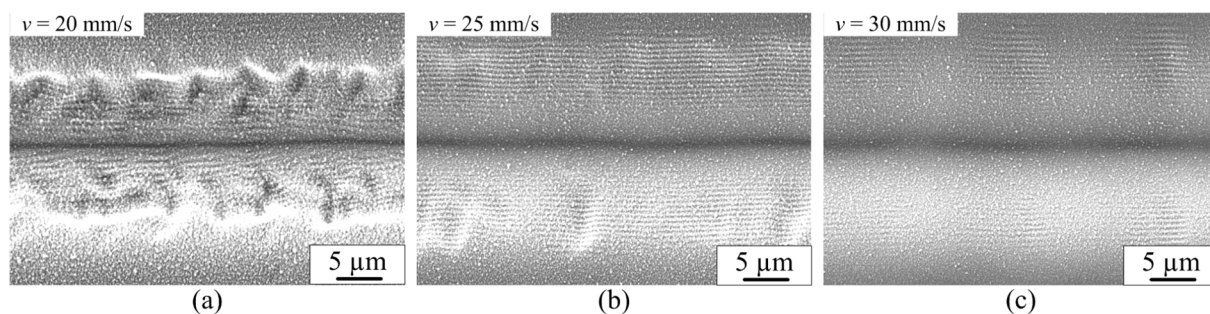


Fig. 6. SEM morphologies of laser irradiated GC surfaces in the middle regions of scanning line under various scanning speeds: (a) 20 mm/s, (b) 25 mm/s, and (c) 30 mm/s. The laser fluence is kept to be 0.235 J/cm^2 .

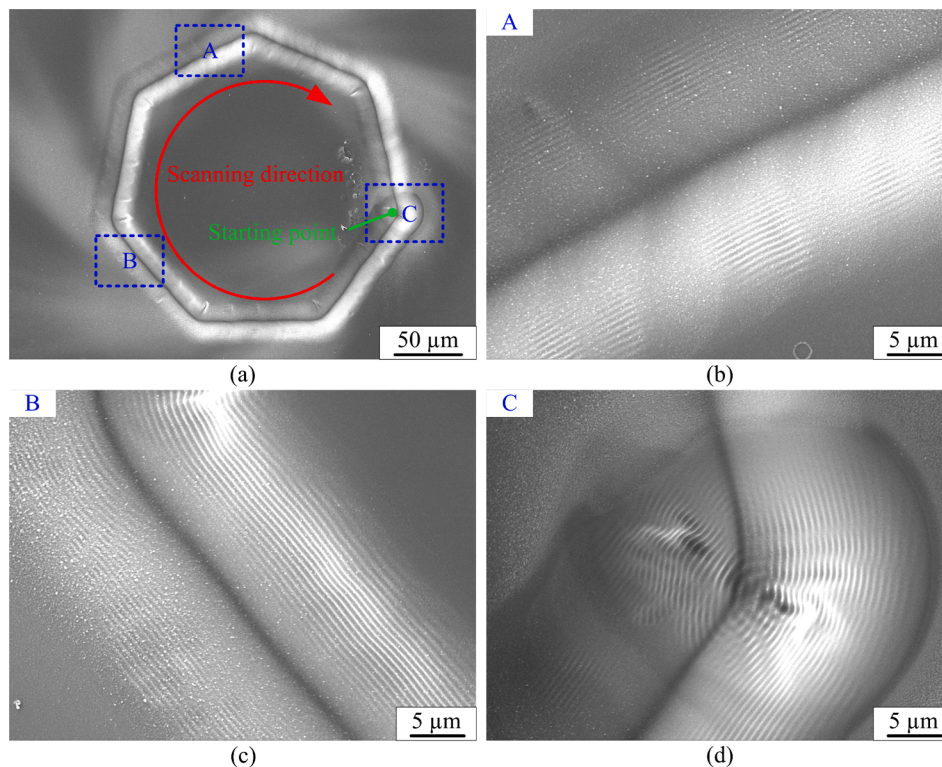


Fig. 7. (a) SEM morphology of the hexagonal structure fabricated on the GC surface by direct line scanning. (b), (c), and (d) are the enlarged images of the regions A, B, and C in Fig. 7a. The laser fluence and scanning speed are kept to be 0.235 J/cm^2 and 25 mm/s , respectively.

homogeneity of micro/nano-structures in various regions is significantly improved, and fewer nanoparticles are deposited in the starting region. In addition, the fluctuation of the cross-sectional profile along the x-axis is reduced, and the uniform profile along the y-axis is still maintained, which further demonstrates the improved uniformity of the linear hierarchical micro/nano-structures. Fig. 10 presents the SEM morphology of the hexagonal structure fabricated on the GC surface by repeated line scanning. It is seen that the well-defined and uniform hexagonal structure could be patterned on the GC surface, and the difference in morphology between the starting and ending regions is significantly eliminated, which verifies the feasibility of the improved method. For comparison, 3D topographies of the hexagonal structures fabricated by direct and repeated line scanning are shown in Fig. 11. It can be seen that the overall uniformity in the depth direction of the hexagonal structure is greatly improved by repeated line scanning. Accordingly, by repeated line scanning with relatively low laser fluence, the micro/nano-structures in various regions of the scanning line are homogenized, and well-defined and uniform hierarchical micro/nano-structures could be obtained by reasonably changing the number of scanning

rather than the laser parameters.

To explore whether the amorphous characteristic of the GC surface had been changed after laser irradiation, the Raman tests were performed on the non-irradiated and irradiated surfaces. Fig. 12 presents the Raman spectra of the GC substrate (Region A) as well as the laser irradiated surface (Region B). Two typical peaks could be observed, the D peak at 1360 cm^{-1} and the G peak at 1590 cm^{-1} . The D peak is associated with defects or disorder and the G peak is related to the graphite and order in carbon material. The intensity ratio I_D/I_G is used to evaluate the degree of amorphization or graphitization of carbon material [30]. As shown in Fig. 12, the ratio I_D/I_G of the substrate surface is about 1.19 ($I_D/I_G > 1$), confirming the amorphous nature of GC substrate [31]. It is clearly seen that the D peak shows a slight high intensity compared to the G peak for the Region B, indicating that the amorphous nature of the GC surface after laser irradiation is well maintained.

4. Conclusions

In summary, this study proposed a method for fabricating linear

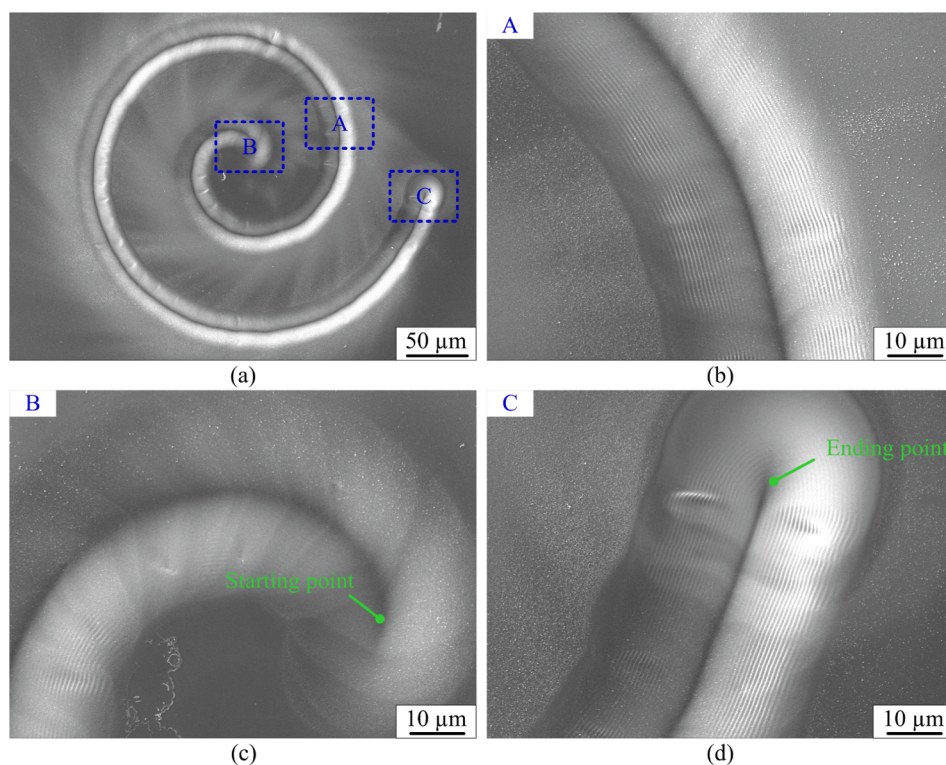


Fig. 8. (a) SEM morphology of the helical structure fabricated on the GC surface by direct line scanning. (b), (c), and (d) are the enlarged images of the regions A, B, and C in Fig. 8a. The laser fluence and scanning speed are kept to be 0.235 J/cm^2 and 25 mm/s , respectively.

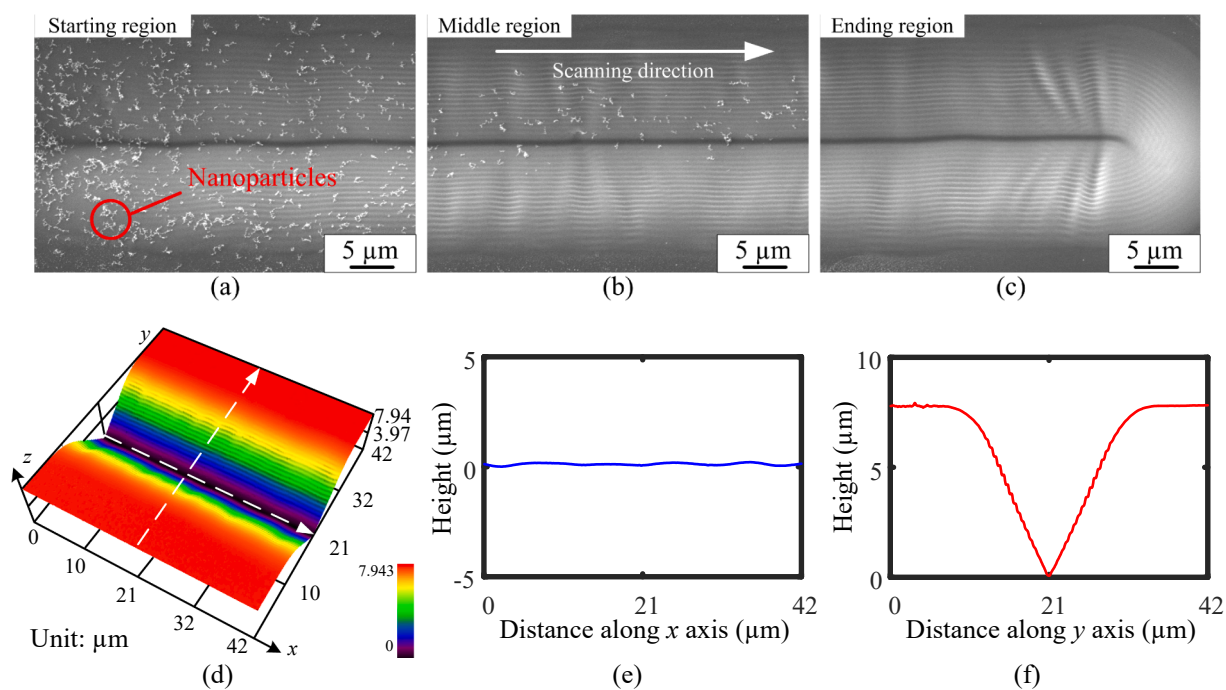


Fig. 9. SEM morphologies of the laser irradiated GC surfaces in various regions of the scanning line by repeated line scanning: (a) starting region, (b) middle region, and (c) ending region. (d) The 3D topography corresponds to the middle region of Fig. 9b and the cross-sectional profiles marked in Fig. 9d along different axes: (e) x-axis, (f) y-axis. The laser fluence, scanning speed, and number of repeated scanning are kept to be 0.182 J/cm^2 , 25 mm/s , and 9, respectively.

hierarchical micro/nano-structures on the GC surface by nanosecond pulsed laser irradiation. By experiments and analysis, the following conclusions could be obtained.

- (1) By tuning the interval between adjacent points as well as the irradiation time, linear hierarchical micro/nano-structures were successfully achieved by point-to-linear conversion. The detailed conversion process and mechanism could be related to the

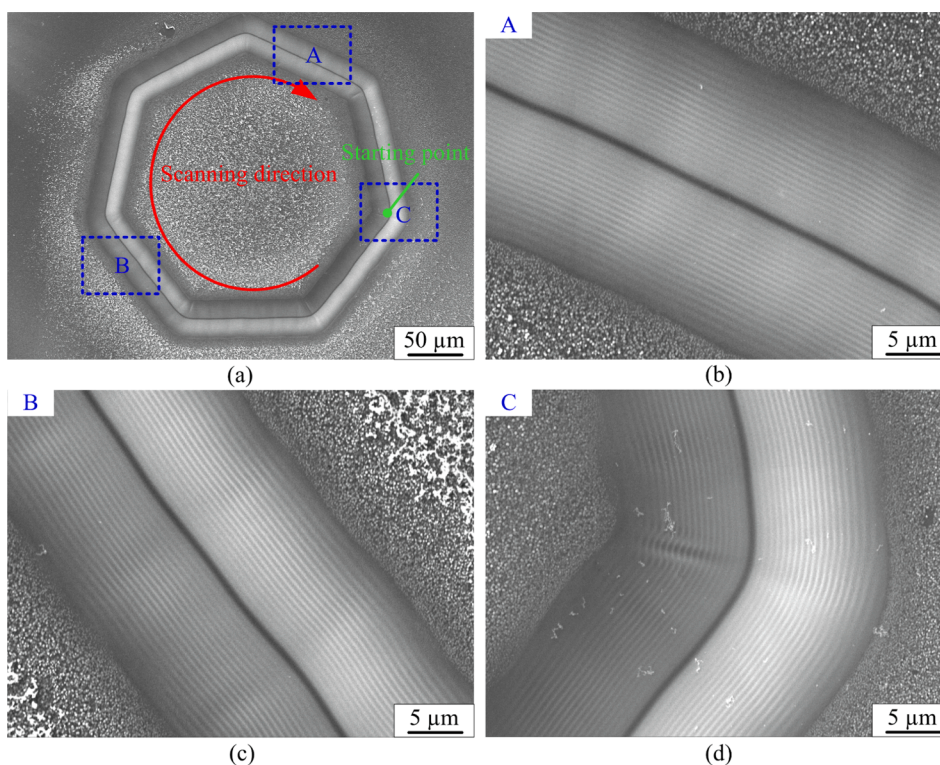


Fig. 10. (a) SEM morphology of the hexagonal structure fabricated on the GC surface by repeated line scanning. (b), (c), and (d) are the enlarged images of the regions A, B, and C in Fig. 10a. The laser fluence, scanning speed, and number of repeated scanning are kept to be 0.182 J/cm^2 , 25 mm/s , and 9 , respectively.

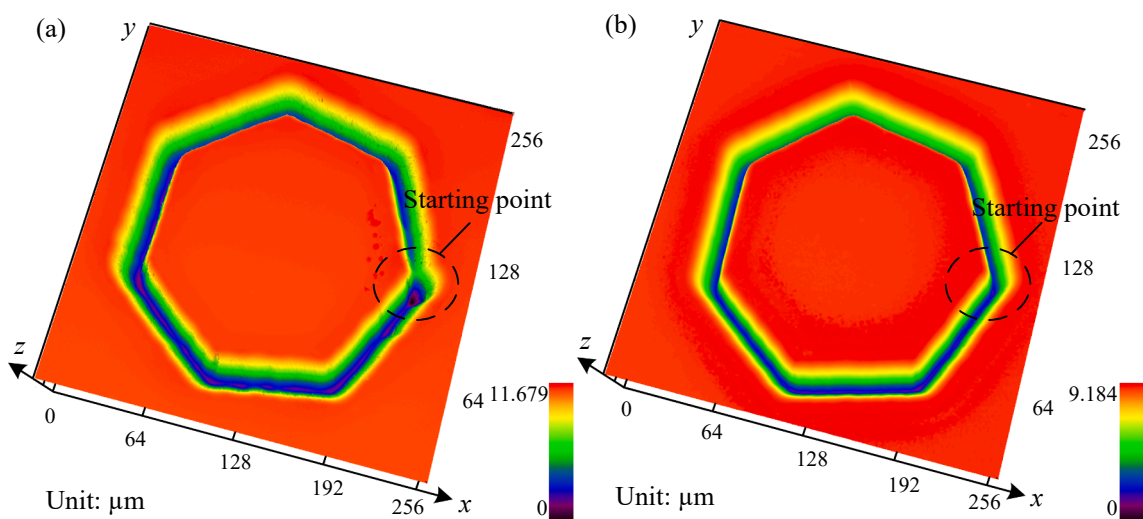


Fig. 11. The 3D topographies of hexagonal structures fabricated by (a) direct and (b) repeated line scanning.

interconnection of branches and internal nanostructures between adjacent point-shape hierarchical micro/nano-structures.

- (2) The linear hierarchical micro/nano-structures with different geometries were fabricated on the GC surface by direct line scanning, and the direction of these structures including the groove and internal nano-gratings was always parallel to the laser scanning direction.
- (3) By repeated line scanning with relatively low laser fluence, the method of direct line scanning was improved, and well-defined and uniform hierarchical micro/nano-structures were fabricated on the GC surface.
- (4) The amorphous nature of structured region on the GC surface was well maintained after laser irradiation.

CRediT authorship contribution statement

Chao Wang: Investigation, Formal analysis, Data curation, Writing – original draft. **Hongyang Zhang:** Investigation, Methodology. **Hu Huang:** Conceptualization, Data curation, Funding acquisition, Methodology, Resources, Supervision, Writing – review & editing. **Zhiyu Zhang:** Investigation. **Lin Zhang:** Investigation. **Jiawang Yan:** Methodology, Supervision.

Declaration of Competing Interest

The authors declare that they have no known competing financial interests or personal relationships that could have appeared to influence

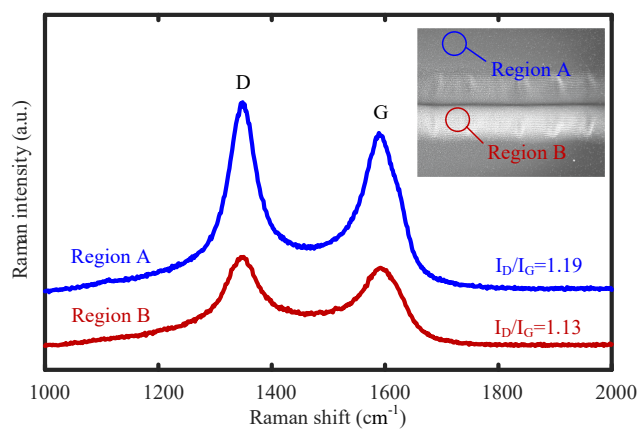


Fig. 12. The Raman spectrums of the GC substrate (Region A) as well as the laser irradiated surface (Region B). The D and G peaks appear at about 1360 cm^{-1} and 1590 cm^{-1} , respectively.

the work reported in this paper.

Acknowledgements

This work was supported by the National Natural Science Foundation of China (Grant No. 51705197), the Graduate Innovation Fund of Jilin University (Grant No. 101832020CX106), and the Fundamental Research Funds for the Central Universities (2019-2022).

References

- [1] L.A. Pesin, Review: structure and properties of glass-like carbon, *J. Mater. Sci.* 37 (2002) 1–28.
- [2] L.d.S. Vieira, A review on the use of glassy carbon in advanced technological applications, *Carbon* 186 (2022) 282–302.
- [3] O.S. Odutemowo, J.B. Malherbe, R. Limbach, L. Wondraczek, E. Wendler, A. Undisz, E.G. Njoroge, D.O. Idisi, M.S. Dhlamini, Changes in the mechanical, structural and electrical properties of glassy carbon due to strontium and silver co-implantation and annealing, *Appl. Surf. Sci.* 537 (2021), 147929.
- [4] A. Harpale, S. Sawant, R. Kumar, D. Levin, H.B. Chew, Ablative thermal protection systems: pyrolysis modeling by scale-bridging molecular dynamics, *Carbon* 130 (2018) 315–324.
- [5] S.A. Adejo, J.B. Malherbe, E.G. Njoroge, M. Mlambo, O.S. Odutemowo, T. Thabethe, Z.A.Y. Abdalla, T.T. Hlatshwayo, Effect of sequential isochronal annealing on the structure and migration behaviour of selenium-ion implanted in glassy carbon, *Vacuum* 182 (2020), 109689.
- [6] F. Simmen, M. Horisberger, B. Seyfang, T. Lippert, P. Novák, M. Döbeli, M. Mallepell, C.W. Schneider, A. Wokaun, Glassy carbon – A promising substrate material for pulsed laser deposition of thin $\text{Li}1+\text{xMn}2\text{O}4-\delta$ electrodes, *Appl. Surf. Sci.* 257 (12) (2011) 5347–5353.
- [7] M. Amare, S. Admassie, Potentiodynamic fabrication and characterization of poly (4-amino-3-hydroxynaphthalene sulfonic acid) modified glassy carbon electrode, *J. Mater. Res. Technol.* 9 (5) (2020) 11484–11496.
- [8] J. Vazquez-Samperio, P. Acevedo-Peña, A. Guzmán-Vargas, E. Reguera, E. Cordoba-Tuta, Incorporation of heteroatoms into reticulated vitreous carbon foams derived from sucrose to improve its energy storage performance, *Inter. J. Energ. Res.* 45 (4) (2020) 6383–6394.
- [9] M. Vomero, E. Castagnola, F. Ciarpella, E. Maggolini, N. Goshi, E. Zucchini, S. Carli, L. Fadiga, S. Kassegne, D. Ricci, Highly stable glassy carbon interfaces for long-term neural stimulation and low-noise recording of brain activity, *Sci. Rep.* 7 (2017) 40332.
- [10] S. Sharma, Glassy carbon: a promising material for micro- and nanomanufacturing, *Materials* 11 (10) (2018) 1–21.
- [11] J. Dukwen, M. Friedrichs, G. Liu, M. Tang, O. Dambon, F. Klocke, Tribological wear analysis and numerical lifetime prediction of glassy carbon tools in fused silica molding, *Wear* 364–365 (2016) 144–153.
- [12] M. Hu, J. He, Z. Zhao, T.A. Strobel, W. Hu, D. Yu, Compressed glassy carbon: an ultrastrong and elastic interpenetrating graphene network, *Sci. Adv.* 3 (2017) 1603213.
- [13] Y.K. Kim, M.R. Haq, S.-M. Kim, Glass molding of all glass Fresnel lens with vitreous carbon micromold, *Opt. Express* 27 (2) (2019) 1553–1562.
- [14] H. Jang, M. Refatul Haq, Y. Kim, J. Kim, P.H. Oh, J. Ju, S.M. Kim, J. Lim, Fabrication of glass microchannel via glass imprinting using a vitreous carbon stamp for flow focusing droplet generator, *Sensors (Basel)* 18 (1) (2017) 1–9.
- [15] S.-W. Youn, A. Ueno, M. Takahashi, R. Maeda, A process of glassy carbon etching without the micro masking effect for the fabrication of a mold with a high-quality surface, *J. Micromech. Microeng.* 19 (12) (2009).
- [16] J. Kim, D. Hong, M.A. Badshah, X. Lu, Y.K. Kim, S.M. Kim, Direct metal forming of a microdome structure with a glassy carbon mold for enhanced boiling heat transfer, *Micromachines (Basel)* 9 (8) (2018) 1–10.
- [17] K. Li, P. Chopra, W. O'Neill, Micromachining of glassy carbon using a Yb-based master oscillator power amplifier nanosecond fiber laser, *Appl. Opt.* 60 (29) (2021) 9082–9086.
- [18] P. Fan, B. Bai, M. Zhong, H. Zhang, J. Long, J. Han, W. Wang, G. Jin, General strategy toward dual-scale-controlled metallic micro-nano hybrid structures with ultralow reflectance, *ACS Nano* 11 (7) (2017) 7401–7408.
- [19] J. Li, W. Wang, X. Mei, A. Pan, X. Sun, B. Liu, J. Cui, Artificial compound eyes prepared by a combination of air-assisted deformation, modified laser swelling, and controlled crystal growth, *ACS Nano* 13 (1) (2019) 114–124.
- [20] D. Wang, Q. Sun, M.J. Hokkanen, C. Zhang, F.-Y. Lin, Q. Liu, S.-P. Zhu, T. Zhou, Q. Chang, B.o. He, Q. Zhou, L. Chen, Z. Wang, R.H.A. Ras, X.u. Deng, Design of robust superhydrophobic surfaces, *Nature* 582 (7810) (2020) 55–59.
- [21] H.H. Nguyen, A.K. Tieu, S. Wan, H. Zhu, S.T. Pham, B. Johnston, Surface characteristics and wettability of superhydrophobic silanized inorganic glass coating surfaces textured with a picosecond laser, *Appl. Surf. Sci.* 537 (2021), 147808.
- [22] Q. Huang, X. Shi, Y. Xue, K. Zhang, C. Wu, Optimization of bionic textured parameter to improve the tribological performance of AISI 4140 self-lubricating composite through response surface methodology, *Tribol. Int.* 161 (2021), 107104.
- [23] C. Wang, H. Huang, Y. Qian, Z. Zhang, J. Yan, One-step fabrication of regular hierarchical micro/nano-structures on glassy carbon by nanosecond pulsed laser irradiation, *J. Manuf. Process* 62 (2021) 108–118.
- [24] V. Narayanan, R. Singh, D. Marla, A computational model to predict surface roughness in laser surface processing of mild steel using nanosecond pulses, *J. Manuf. Process* 68 (2021) 1880–1889.
- [25] S. Faas, U. Bielke, R. Weber, T. Graf, Prediction of the surface structures resulting from heat accumulation during processing with picosecond laser pulses at the average power of 420 W, *Appl. Phys. A-Mater.* 124 (9) (2018).
- [26] R. Weber, T. Graf, C. Freitag, A. Feuer, T. Kononenko, V.I. Konov, Processing constraints resulting from heat accumulation during pulsed and repetitive laser materials processing, *Opt. Express* 25 (4) (2017) 3966–3979.
- [27] Y.Q. Xing, L. Liu, Z. Wu, X.S. Wang, P. Huang, L. Tang, Fabrication and characterization of micro-channels on $\text{Al}_2\text{O}_3/\text{TiC}$ ceramic produced by nanosecond laser, *Ceram. Int.* 44 (18) (2018) 23035–23044.
- [28] C. Wang, H. Huang, Y. Qian, Z. Zhang, W. Huang, J. Yan, Nitrogen assisted formation of large-area ripples on Ti6Al4V surface by nanosecond pulse laser irradiation, *Precis. Eng.* 73 (2022) 244–256.
- [29] B. Liu, B.-Q. Li, Z. Li, P. Bai, Y. Wang, Z. Kuai, Numerical investigation on heat transfer of multi-laser processing during selective laser melting of AISI10Mg, *Results Phys.* 12 (2019) 454–459.
- [30] A. Ferrari, J. Robertson, S. Reich, C. Thomsen, Raman spectroscopy of graphite, *Philos. T. R. Soc. A.* 362 (1824) (2004) 2271–2288.
- [31] S.M. Taylor, A. Pătru, D. Streich, M. El Kazzi, E. Fabbri, T.J. Schmidt, Vanadium (V) reduction reaction on modified glassy carbon electrodes – Role of oxygen functionalities and microstructure, *Carbon* 109 (2016) 472–478.